JOURNAL OF SOLID STATE CHEMISTRY 119, 24–35 (1995)

# Magnetic and Transport Properties of $CeVO_3$

Hoan C. Nguyen and John B. Goodenough

*Center for Materials Science and Engineering, ETC 9.102, The University of Texas at Austin, Austin, Texas 78712-1063*

Received December 1, 1994; in revised form March 8, 1995; accepted March 13, 1995

**Magnetic data are presented that indicate the $VO_3$ array of the perovskite $CeVO_3$ exhibits the same anomalous properties as in $LaVO_3$, including (1) a first-order magnetostrictive distortion below a $T_t < T_N$, (2) a canted-spin ferromagnetism below $T_N$, (3) a reversal of the direction of the vanadium atomic moments on traversing $T_t$, and (4) suppression of $T_t$ in an isostructural metastable phase prepared under hydrostatic pressure. The V–Ce exchange field operating at the $Ce^{3+}:4f^1$ configurations below $T_N$ does not change sign on traversing $T_t$. The Ce-atom magnetization reduces the field for nucleation of irreversible magnetization processes; both $La_{0.5}Ce_{0.5}VO_3$ and $CeVO_3$ exhibit $M$–$H$ hysteresis loops characteristic of hard ferromagnets, whereas the magnetization of $LaVO_3$ remains reversible in fields $H = \pm 50$ kOe. For $x \geq 0.25$, substitution of Sr for Ce in $Ce_{1-x}Sr_xVO_3$ does not create small-polaron $V^{4+}$ ions, but delocalized V-3*d* states and an intermediate $Ce^{4+}/Ce^{3+}$ valence at the Ce atoms. Strong correlations among the itinerant V-$\pi^*$ electrons of stoichiometric, metallic $SrVO_3$ reintroduce long-range magnetic order at low temperatures.** © 1995 Academic Press, Inc.

## INTRODUCTION

The orthorhombic (space group *Pbnm*) perovskite $LaVO_3$ undergoes a first-order decrease of its axial ratio $c/\sqrt{2}a$ on cooling through a transition temperature $T_t \approx 138$ K $< T_N \approx 142$ K (1, 2); the magnetic order below $T_t$ has a canted-spin configuration $C_yF_x$ with a ferromagnetic component along the **a** axis of the orthorhombic cell (1). A later refinement shows a distortion to monoclinic $P2_1/a$ symmetry below $T_t$, in which the ferromagnetic component is along the **b** axis of the monoclinic cell with a rhombohedral component to the distortion of the $V^{3+}$ octahedra (3, 4). The notation $C_yF_x$ for the magnetic order has been defined by Bertaut (5).

If polycrystalline $LaVO_3$ is cooled or quenched from 300 to 4 K in zero magnetic field (ZFC or ZFQ case), the magnetic susceptibility measured in 1 kOe looks like that of a Néel antiferromagnet; cooling in zero field leaves the compound demagnetized, and only reversible magnetization processes occur in an applied field of 1 kOe. However, cooling or quenching in an applied field of 1 kOe from 300 to 4 K (FC-1 kOe or FQ-1 kOe case) gives rise to an "anomalous diamagnetism" below $T_t$ if the measurements are made on heating in the same applied field as on cooling (6, 7). We have shown experimentally that this anomalous diamagnetism reflects an orientation of the canted-spin ferromagnetism in opposition to the magnetizing field on cooling through the first-order transition temperature $T_t$ (6, 7). We have argued (6, 7) that the first-order transition is due to a Jahn–Teller distortion that enhances the orbital angular momentum discontinuously by an amount $\Delta L$, thereby inducing a persistent atomic current that opposes the magnetizing field and consequently reversing each total $V^{3+}$-ion atomic moment $\mu_V$ due to intraatomic spin-orbit coupling. In support of this argument, we showed that suppression of the first-order magnetostrictive distortion at $T_t$ eliminates the anomalous diamagnetism.

The magnetostrictive distoriton is suppressed by applying pressure on the $(VO_3)^{3-}$ array; a hydrostatic pressure $P \geq 8$ kbar stabilizes a metastable isostructural high-pressure $LaVO_3$ phase and chemical pressure stabilizes an isostructural $YVO_3$ phase that does not form a solid solution with ambient-pressure $LaVO_3$ [7]. With the exception of Ce, substitution of smaller rare-earth atoms for La suppresses the first-order magnetostrictive distortion at $T_t$. $CeVO_3$ retains a magnetostrictive distortion like that found in $LaVO_3$ with $T_t \approx 124$ K $< T_N \approx 136$ K; it also has the same $C_yF_x$ magnetic structure (referred to as orthorhombic *Pbnm* symmetry) as $LaVO_3$ below $T_t$ (1). Therefore, we have investigated $CeVO_3$ to determine whether there is evidence in this compound also for an anomalous diamagnetism of the $VO_3$ array after or with a FC-1 kOe. In addition, we explore the system $Ce_{1-x}Sr_xVO_3$. We show that a semiconductor–metal transition occurs at the Sr-atom percolation limit, as in $La_{1-x}Sr_xO_3$, and the $Ce^{3+}$ valence of $CeVO_3$ is transformed to an intermediate-valence state on oxidation of the $(VO_3)^{3-}$ array; the $VO_3$-$\pi^*$ band apparently overlaps the $Ce^{4+}/Ce^{3+}$ couple in the metallic phase.

## EXPERIMENTAL PROCEDURES

Polycrystalline $Ce_{1-y}La_yVO_{4+z}$ and $Sr_2V_2O_7$ were first prepared by standard solid-state reaction in air at 850°C from stoichiometric mixtures of $CeO_2$, $La_2O_3$, $SrCO_3$,



0022-4596/95 $12.00

and $V_2O_5$. The powdered $Sr_2V_2O_7$ and $Ce_{1-y}La_yVO_{4+z}$ were fired in flowing hydrogen at 800 and 1100°C, respectively, to reduce them to $SrVO_3$ and $Ce_{1-y}La_yVO_3$. Finally, polycrystalline $Ce_{1-x}Sr_xVO_3$ samples were prepared by solid-state reaction in ultrapure argon at 1400°C from a mixture of $CeVO_3$ and $SrVO_3$ with several intermittent regrindings and refirings. Samples that were single-phase to X-ray powder diffraction, taken with a Philips diffractometer and Cu$K\alpha$ radiation, were pressed and sintered at 1400°C in ultrapure argon. The X-ray diffraction peak positions were calibrated against Si as an internal standard, and the lattice parameters were obtained with a least-squares fitting procedure. The oxygen content of selected samples was determined by thermogravimetric analysis on oxidation to $V_2O_5$, $CeO_2$, and $La_2O_3$.

X-ray photoelectron spectroscopy (XPS) was used to monitor the evolution with $x$ of the valence of the vanadium and cerium ions in the system $Ce_{1-x}Sr_xVO_3$. Data were obtained at room temperature with a VG ESCALAB MARK I spectrometer having a base pressure less than $10^{-7}$ Torr and employing monoenergetic Mg$K\alpha$ X-ray radiation (1253.6 eV). The X-ray anode was operated at 330 W. The photoelectrons were detected with an electron multiplier tube and an EA-11 hemispherical analyzer operated at a constant pass energy of 50 eV. The surface of the sample was mounted normal to the axis of the analyzer entrance aperture. The depth of sample probed in such an oxide is under 25 Å.

Magnetic susceptibility was measured between 5 and 300 K with a SQUID magnetometer in applied fields $-50 \leq H \leq 50$ kOe. The resistance of polycrystalline samples was measured with a four-probe technique; it was corrected for a thermoelectric contribution by subtracting the off-current background. The thermopower was measured by the dc method with an experimental system described elsewhere (8); a temperature difference $\Delta T = 5$ K across the sample was used for each Seebeck measurement.

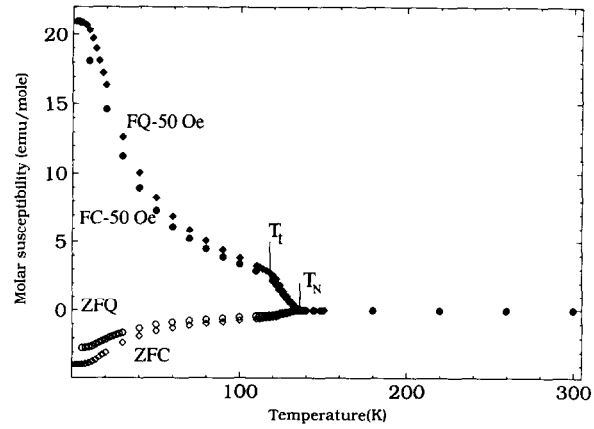


FIG. 1. Temperature dependence of the molar susceptibility of $CeVO_3$ taken in 50 Oe after ZFC or ZFQ and FC-50 Oe or FQ-50 Oe from room temperature to 4 K.

## EXPERIMENTAL RESULTS

*1. Structure.* The perovskite systems $Ce_{1-y}La_yVO_3$ and $Ce_{1-x}Sr_xVO_3$ remain orthorhombic, space group *Pbnm*, at room temperature and appear to form complete solid solutions over the ranges $0 \leq y \leq 0.5$ and $0 \leq x \leq 1.0$, respectively. The room-temperature volume of the system $Ce_{1-x}Sr_xVO_3$ decreases with $x$ over the compositional range $0.25 \leq x \leq 0.75$, see Table 1; the volume change does not obey Végard's law, and $SrVO_3$ expands discontinuously as the oxygen content is increased from 2.9 to 3.0 per formula unit.

*2. $CeVO_3$.* Figure 1 shows the magnetic susceptibility of $CeVO_3$ taken in 50 Oe on heating from 4 to 300 K after a FC-50 Oe and a FQ-50 Oe as well as a ZFC and a ZFQ. Both $T_N$ and $T_t$ are evident, particularly in the FC and FQ curves.

After the ZFC and ZFQ treatments, the sample was not fully demagnetized; it had a net residual magnetization

TABLE 1

**Room Temperature Lattice Parameter, Curie Constant, Neél Temperature, Magnetostrictive Transition Temperature and Curie Paramagnetic Temperature $\Theta_p$ of $Ce_{1-y}La_yVO_3$ and $Ce_{1-x}Sr_xVO_3$**

| Samples | $a$ (Å) | $b$ (Å) | $c$ (Å) | $V$ (Å)$^3$ | $\Theta_p$ (−K) | $C_M$ (emu/Kmole) | $T_N$ (K) | $T_t$ (K) |
|---|---|---|---|---|---|---|---|---|
| $LaVO_3$ | 5.547 | 5.546 | 7.842 | 241.23 | 670 | 1.60 | 142 | 138 |
| $Ce_{0.5}La_{0.5}VO_3$ | 5.531 | 5.546 | 7.822 | 239.95 | 257 | 1.56 | 135 | 124 |
| $CeVO_3$ | 5.519 | 5.544 | 7.805 | 238.11 | 158 | 1.74 | 125 | 124 |
| $Ce_{0.75}Sr_{0.25}VO_3$ | 5.514 | 5.560 | 7.794 | 238.94 | 219 | 1.38 | | |
| $Ce_{0.50}Sr_{0.50}VO_3$ | 5.437 | 5.649 | 7.775 | 238.79 | 222 | 0.86 | | |
| $Ce_{0.25}Sr_{0.75}VO_3$ | 5.519 | 5.550 | 7.779 | 238.26 | 249 | 0.46 | | |
| $SrVO_3$ | 5.367 | 6.156 | 7.701 | 254.40 | non-Curie–Weiss | | | |
| $SrVO_{2.9}$ (cubic) | 3.842 | | | | Pauli paramagnetic | | | |

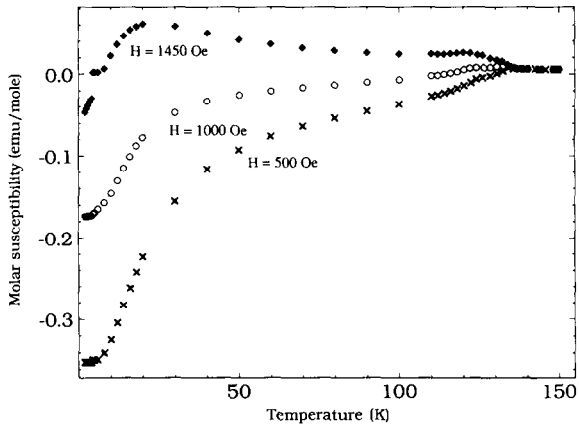


FIG. 2. Temperature dependence of the molar susceptibility of $CeVO_3$ measured in $H$ = 500, 1000, or 1450 Oe after ZFC from room temperature to 4 K.

in four out of five experiments performed. The measuring field used for Fig. 1 was applied in opposition to the residual magnetization, which was greater after a ZFC than a ZFQ treatment.

The FC and FQ measurements of Fig. 1 were made with the magnetic field $H$ = 50 Oe applied in the same direction as during cooling. Below $T_N \approx 136$ K, the $V^{3+}$ ions have the same canted-spin arrangement as in $LaVO_3$ below a $T_N \approx 142$ K, and the $4f^1$ configuration at a $Ce^{3+}$ ion experiences an exchange field that is stronger than the applied field. The V–Ce exchange field enhances the contribution to the magnetization coming from the Ce-atom array. In the interval $T_t \approx 124$ K $< T < T_N \approx 136$ K, the contributions from both the $V^{3+}$-ion and $Ce^{3+}$-ion arrays appear to add to the total magnetization **M** oriented in the direction of **H**. The slope $d\chi_m/dT$ changes abruptly at $T_t$; this change may reflect an enhanced magnetocrystalline anisotropy below $T_t$, but it could also signal a reversal of the magnetization of the $VO_3$ array as occurred below the $T_t$ of $LaVO_3$ in a FC experiment. Evidently any reversal in the sign of the $V^{3+}$-ion contribution to the magnetization does not change the sign of the Ce-atom contribution. Below 40 K, the V–Ce atom interactions clearly enhance the Ce-atom magnetic ordering and hence their contribution to the magnetization as temperature decreases.

Figure 2 shows measurements taken on a ZFC sample in $H$ = 500, 1000, and 1450 Oe applied in a direction opposite to the residual magnetization at 4 K. In this case also, the slope $d\chi_m/dT$ changes abruptly at $T_t$ as in the FC and FQ experiments. The net magnetization exhibits an increasing change in the direction of **H** with increasing field strength and temperature, particularly below 20 K. At 20 K, a critical field for the reversal of the magnetization is $H \approx 1.2$ kOe.

Figure 3 shows an abrupt change in the magnetic susceptibility of a ZFC sample at a spin-reorientation temperature $T_s \approx 4$ K; the magnetic transition temperature does not change with increasing strength of the measuring field. This transition probably reflects a spin reorientation of the Ce-atom array.

The evolution with temperature of $\chi_m(T)$ for different measuring fields $H$ = 50, 100, 150, 350, 400, 1000, 50,000 Oe after a ZFQ, Fig. 4, is similar to that after a ZFC treatment. With lower measuring fields, the change in $d\chi_m/dT$ at $T_t$ is particularly marked; it even changes sign, which supports the hypothesis that the sign of the magnetization of the $VO_3$ array is changing without a change in sign of the contribution from the Ce-atom array. At 10 K, the net magnetization reverses sign in a field $H \approx$ 350 Oe.

Figure 5 shows a $\chi_m(T)$ curve taken in an $H$ = 1 kOe after a ZFQ at 80 K; the twin maxima occur at $T_t$ and $T_N$.

In order to test whether the magnetization **M** exhibits an $M$–$H$ hysteresis loop in $CeVO_3$, in contrast to the observation for $H \leq 50$ kOe of almost all reversible magnetization processes in $LaVO_3$, we measured $M$ versus $H$ at 20 K after a FC-1 kOe to 20 K for $CeVO_3$, $Ce_{0.5}La_{0.5}VO_3$ and $LaVO_3$. The results for an excursion $-50 \leq H \leq 50$ kOe are displayed in Fig. 6. As can be seen, the magnetization processes for the $VO_3$ array of $LaVO_3$ are completely reversible; there is no opening of the curve characteristic of magnetic hysteresis, but an $M < 0$ is found for $H < 3$ kOe. With $H < 3$ kOe the $VO_3$ array has a magnetization opposed to the applied field, and the individual atomic moments $\mu_V$ are strongly held to their zero-field orientations by a giant magnetocrystalline anisotropy, a consequence of the magnetostrictive Jahn–Teller distortion below $T_t$. In contrast, $CeVO_3$ and $Ce_{0.5}La_{0.5}VO_3$ exhibit hysteresis loops typical of a hard ferromagnet with a saturation magnetization that increases with the concentration of Ce atoms.

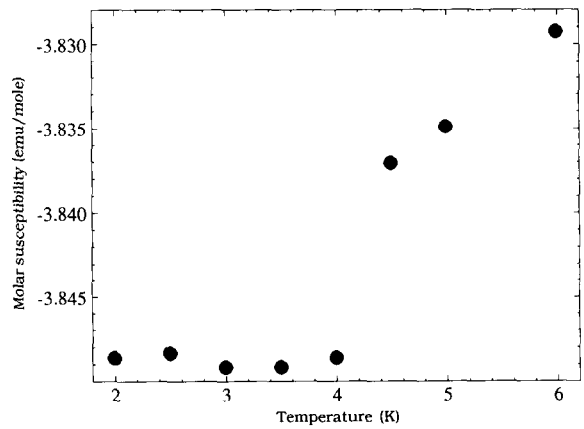


FIG. 3. Temperature dependence of the molar susceptibility for $CeVO_3$ measured in $H$ = 50 Oe between 2 and 6 K after ZFC from room temperature to 2 K.

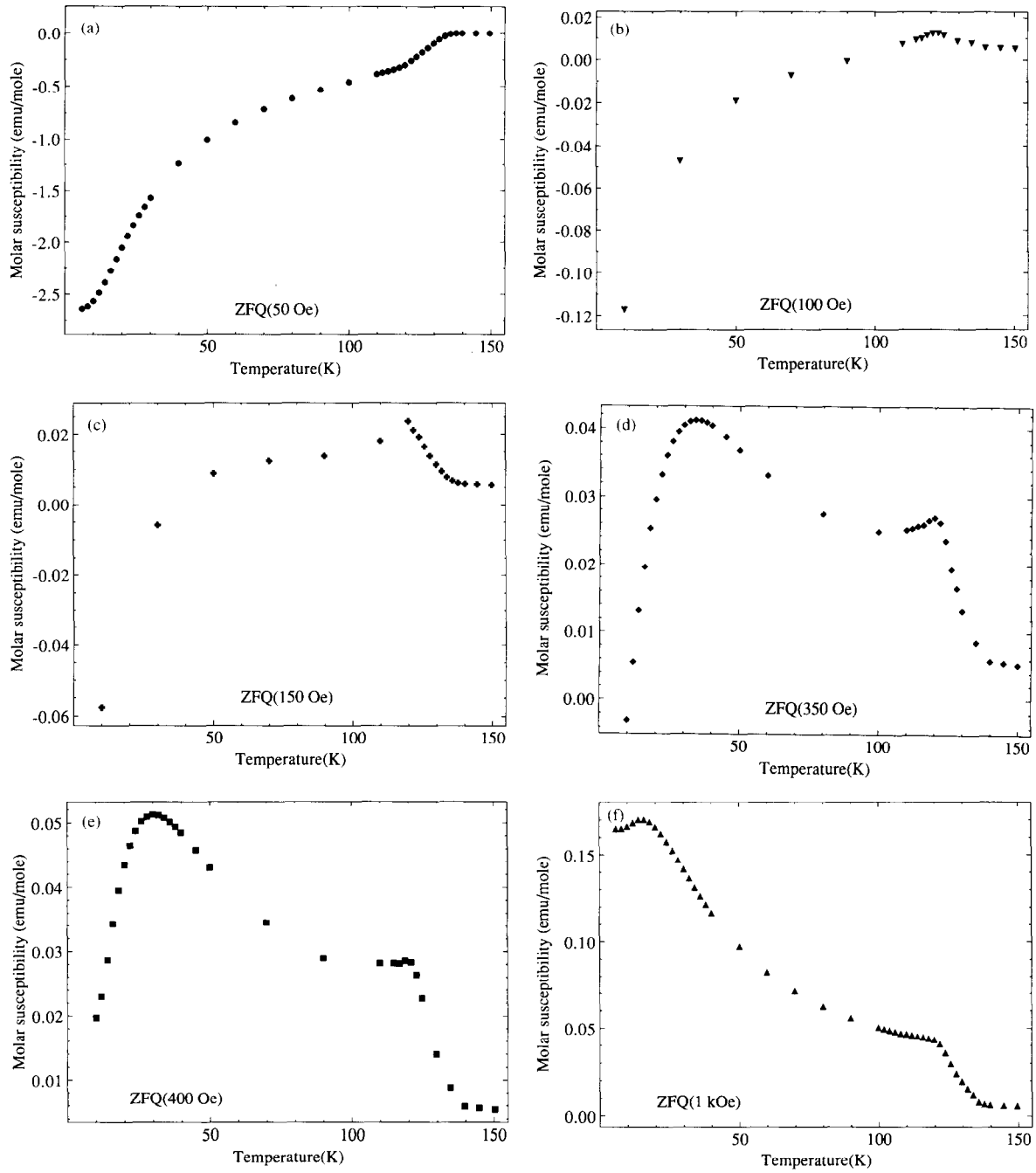


FIG. 4. Temperature dependence of the molar susceptibility of $CeVO_3$ measured in $H$ = 50, 100, 150, 350, 400, 1000, and 50,000 Oe after ZFQ from room temperature to 4 K.

Figure 7 shows the evolution with temperature of the $M(H)$ hysteresis loops for a sample FC-1 kOe and FC-50 kOe to the measuring temperature at 20 K. The evolution with temperature of the $M$–$H$ hysteresis loop is typical of a hard ferromagnet, as can be seen from the evolution of the coercivity and remanence plotted in Fig. 8.

As for $LaVO_3$, preparation of a sample of $CeVO_3$ at 30 kbar with pressure release at room temperature results in an isostructural high-pressure $CeVO_3$ that is metastable at room temperature. Although the unit-cell volume does not change significantly, differential thermal analysis revealed a conversion back to the atmospheric-pressure phase occurring below 400°C as in high-pressure $LaVO_3$. Figure 9a compares the $\chi_m(T)$ curves for the two phases

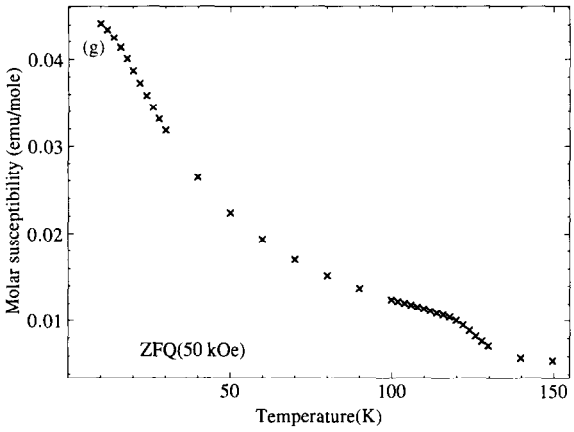


FIG. 4—*Continued*

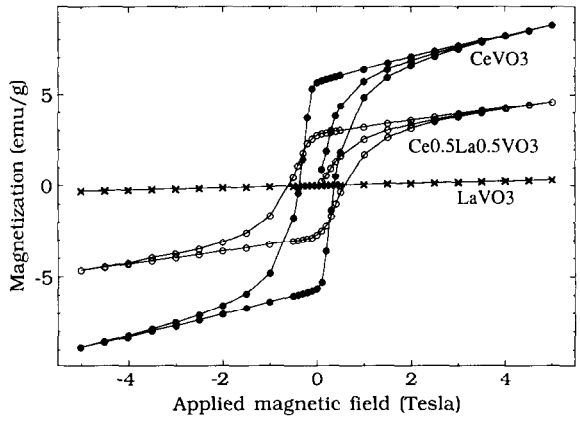


FIG. 6. $M(H)$ curves of $Ce_{1-y}La_yVO_3$ taken at 20 K after ZFC from room temperature to 20 K.

taken in 1 kOe after a FC-1 kOe treatment. The high-pressure phase of $LaVO_3$ is antiferromagnetic with little change in $T_N$, but without weak ferromagnetism and without a magnetostrictive distortion. The high-pressure $CeVO_3$ has a smaller $\chi_m(T)$ below $T_N$ than the atmospheric-pressure phase, which indicates that the $VO_3$ array is behaving as it does in high-pressure $LaVO_3$ where there is no anomalous diamagnetism. Stabilization of a metastable high-pressure $LnVO_3$ phase was not found for smaller lanthanide ions $Ln^{3+}$; comparison of $\chi_m(T)$ obtained in 1 kOe after a FC-1 kOe treatment for $PrVO_3$ and $CeVO_3$ shows, Fig. 9b, no sharp break in $d\chi_m/dT$ at $T_t$ in $PrVO_3$.

*3. $Ce_{1-x}Sr_xVO_3$.* Comparison of the system $Ce_{1-x}Sr_xVO_3$ with $La_{1-x}Sr_xVO_3$ is useful. Mahajan *et al.* (9) have monitored the evolution with $x$ of the room-temperature structure as well as the magnetization $M(T)$ and resistance $R(T)$ behavior of the system $La_{1-x}Sr_xVO_3$. Their data showed a linear decrease with $x$ of the volume of the orthorhombic cell, the smaller size of a $V^{4+}$ ion versus a $V^{3+}$ ion outweighing the larger size of a $Sr^{2+}$ ion versus a $La^{3+}$ ion. Their data also indicated that, for $x > 0.3$, the conduction electrons occupy a strongly exchange-enhanced, narrow $d$ band; they found no evidence from NMR data of either antiferromagnetic spin fluctuations or superconductivity in the metallic phase.

Figure 10 shows the evolution of the resistance $R(T)$ with $x$ for the system $Ce_{1-x}Sr_xVO_3$. Like $LaVO_3$, $CeVO_3$ is an insulator. At $x = 0.25$, the extrinsic conduction exhibits a small activation energy; a transition to metallic behavior occurs in the interval $0.25 < x < 0.5$ as in the $La_{1-x}Sr_xVO_3$ system. However, at $x = 0.5$ the $R(T) \sim T$ behavior is characteristic of a narrow $d$ band with strong electron–phonon interactions; it is only at $x \geq 0.75$ that the $R(T)$ curve has the $T^2$ dependence typical of a Fermi liquid. A similar evolution was found (9) in the system $La_{1-x}Sr_xVO_3$.

The Seebeck data of Fig. 11 show evidence of a gradual transition from two-carrier to single-carrier conduction with increasing $x$.

The inverse magnetic susceptibility for $0.25 \leq x \leq 0.75$, see Fig. 12a, exhibits a Curie–Weiss law at high temperatures, no evidence of a magnetic-ordering temperature, and a low-temperature dependence typical of an intermediate-valence system (10). The system $La_{1-x}Sr_xVO_3$ exhibits a temperature-independent, Stoner-enhanced Pauli paramagnetism in the range $0.2 \leq x \leq 0.9$, the enhancement factor decreasing with increasing $x$ (9). On the other hand, the end member $SrVO_3$ exhibits a higher susceptibility if FC-1 kOe than if ZFC, particularly below 190 K, see Fig. 12b.

After subtracting the monochromatic O-1*s* contribution, the room-temperature XPS data, Fig. 13, show no evidence of two valence states on either the V-atom or Ce-atom arrays, but rather a continuous shifting of the

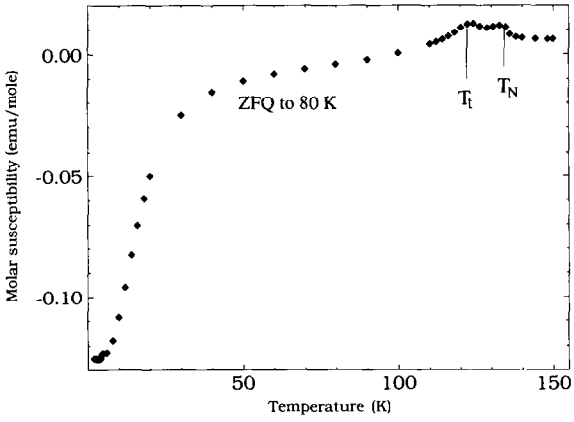


FIG. 5. Temperature dependence of the molar susceptibility of $CeVO_3$ measured in 1000 Oe after ZFQ from room temperature to 80 K.

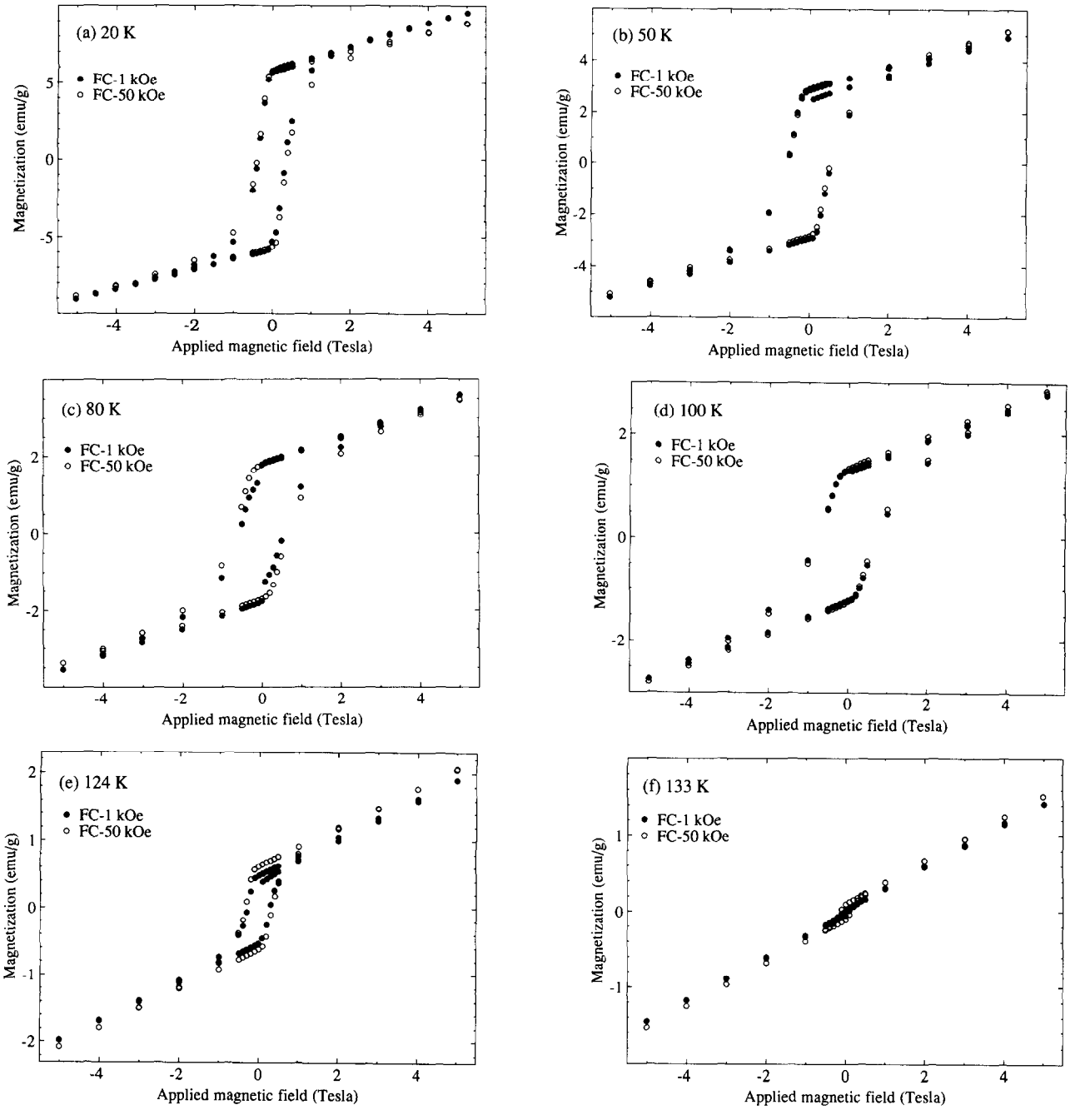


FIG. 7. $M(H)$ curves of $CeVO_3$ taken at $T_a$ = 20, 50, 80, 100, 124, and 133 K after FC-1 kOe and FC-50 kOe from room temperature to $T_a$ ($T_a$ refers to temperature at which the applied field is varied).

core-electron binding energies to lower values with increasing $x$, see Table 2.

## DISCUSSION

*1. $CeVO_3$.* The magnetization **M** of $CeVO_3$ contains two components, one from the Ce-atom array, one from the V-atom array:

$$\mathbf{M} = \mathbf{M}_{Ce} + \mathbf{M}_{V}. \quad [1]$$

Like $LaVO_3$, the orthorhombic perovskite $CeVO_3$ undergoes a first-order contraction of the $c/\sqrt{2}a$ ratio on cooling through the magnetostrictive transition temperature $T_t < T_N$. The magnetostrictive distortion arises from a cooperative Jahn–Teller distortion that removes the threefold orbital degeneracy of the octahedral-site $^3T_{1g}$

TABLE 2
Core-Binding Energies (BE) of Ce-3*d*, V-2*p*, and O-1*s* for $Ce_{1-x}Sr_xVO_3$ (All Data in eV)

| Sample | Ce-3*d* $3d_{5/2}$ | $3d_{3/2}$ | V-2*p* $2p_{3/2}$ | $2p_{1/2}$ | O-1*s* 1*s* |
|---|---|---|---|---|---|
| $CeVO_3$ | 889.8 | 908.3 | 520.7 | 528.5 | 534.0 |
| $Ce_{0.75}Sr_{0.25}VO_3$ | 889.3 | 908.0 | 520.3 | 528.0 | 533.7 |
| $Ce_{0.50}Sr_{0.50}VO_3$ | 889.0 | 907.0 | 520.0 | 527.5 | 533.2 |
| $Ce_{0.50}Ca_{0.50}VO_3$ | 889.2 | 907.5 | 520.1 | 527.5 | 533.2 |
| $Ce_{0.25}Sr_{0.75}VO_3$ | 887.3 | 905.9 | 518.3 | 525.5 | 531.5 |
| $Ce_2O_3$ [a] | 885.3 | 903.8 | | | 530 |
| $CeO_2$ [a] | 882.1 | 900.6 | | | 528 |
| V [b] | | | 512.4 | 519.9 | |
| $V_2O_3$ [b] | | | 515.7 | 523.3 | 530.1 |
| $VO_2$ [b] | | | 515.9 | 523.3 | 529.7 |

[a] From (18–21).
[b] From (21, 22).

configuration at the $V^{3+}$ ions, but with a sign that enhances the orbital angular momentum and allows a strong spin-orbit coupling to remove the remaining orbital degeneracy. Such a distortion can be cooperative only below a long-range magnetic-ordering temperature, which is why we find $T_t < T_N$. The cooperative distortion introduces a giant magnetocrystalline anisotropy that would hold the orientation of an individual vanadium moment $\mu_V$ to the local principal axis of its distorted octahedral site, which is why the magnetization of the canted-spin ferromagnet $LaVO_3$ only changes reversibly in field strengths $H \leq 50$ kOe. Moreover, a first-order transition at $T_t$ introduces a discontinuous change in the orbital angular momentum; we have postulated that this discontinuous change is responsible for a reversal in the sign of $\mathbf{M}_V$ in $LaVO_3$.

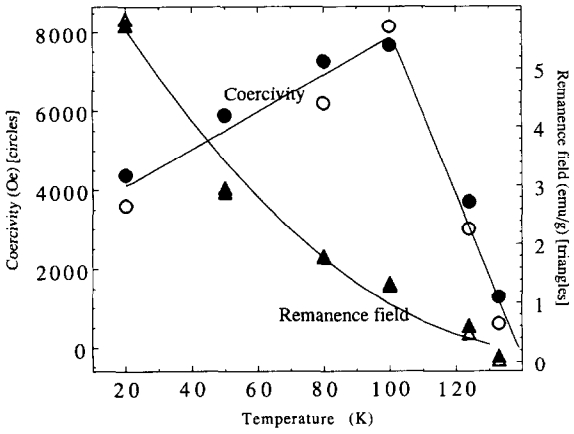


FIG. 8. Coercivity (circles) and remanence (triangles) of $M(H)$ curves for $CeVO_3$ after Fig. 7 with FC-1 kOe (open data points) and FC-50 kOe (closed data points). Solid lines are drawn as guides to the eye.

Since a similar crystallographic change is observed at $T_t$ in $CeVO_3$, we can expect the $VO_3$ array in this compound to exhibit properties similar to those of the $VO_3$ array in $LaVO_3$. The magnetic data of Figs. 1 and 2 provide indirect evidence that $\mathbf{M}_V$ reverses sign on heating/cooling through $T_t$ just as in $LaVO_3$.

The observation that $\mathbf{M}_{Ce}$ does not change sign when $\mathbf{M}_V$ changes sign would indicate that the exchange field operative at the Ce: $4f^1$ configuration due to the Ce–V interactions is predominantly antisymmetric and oriented perpendicular to the vanadium-atom moments,

$$\mathbf{H}^{ex}_{Ce-V} \sim \mu_{Vi} \times \mu_{Vj}, \qquad [2]$$

where $\mu_{Vi}$ and $\mu_{Vj}$ belong to the two different vanadium subarrays of the canted-spin configuration. A reversal of the sign of the $\mu_V$ would not change the sign of the exchange field of Eq. [2]. An orientation of the rare-earth atomic moments perpendicular to the transition-metal moment in $LnMO_3$ perovskites ($Ln$ = rare earth, $M$ = transition metal) is common (11).

The observation of a symmetric $M$–$H$ hysteresis loop, Fig. 6, implies an irreversible growth of favorably oriented magnetic domains in a field $H > H_N$, where the field $H_N$ at the knee of the hysteresis loop is the field required for the nucleation and/or irreversible growth of favorably oriented magnetic domains. The coupling of $\mathbf{H}$ to $\mathbf{M}_{Ce}$ and of $\mathbf{M}_{Ce}$ to $\mathbf{M}_V$ is apparently strong enough to force an irreversible domain-wall motion in $CeVO_3$, whereas a field $H = 50$ kOe is not large enough to induce domain-wall nucleation and/or growth in $LaVO_3$. A larger saturation magnetization $M_s$ in $CeVO_3$ would lower the field $H_N$ for nucleation of domains of reverse magnetization (12, 13),

$$H_N = \frac{2K_1}{M_s}\alpha_K\alpha_\psi - N_{eff}M_s, \qquad [3]$$

where $K_1$ is an effective magnetocrystaline anisotropy constant, $N_{eff}$ is an effective demagnetization factor, and $\alpha_K\alpha_\psi$ is an extrinsic parameter.

We can obtain an estimate of the variation of the effective $K_1$ from the hysteresis loops of Fig. 6. For a hard magnet, the initial magnetization curve is described by the empirical formula (14–17)

$$M = M_s\left(1 - \frac{a}{H} - \frac{b}{H^2}\right) + \chi_0 H, \qquad [4]$$

where $\chi_0 = (dM/dH)_{rev}$ is the contribution arising from reversible rotations of the $\mu_V$ against their local crystalline-anisotropy and exchange fields. A value for $\chi_0$ is obtained from the slope of the $M(H)$ curve found on decreas-

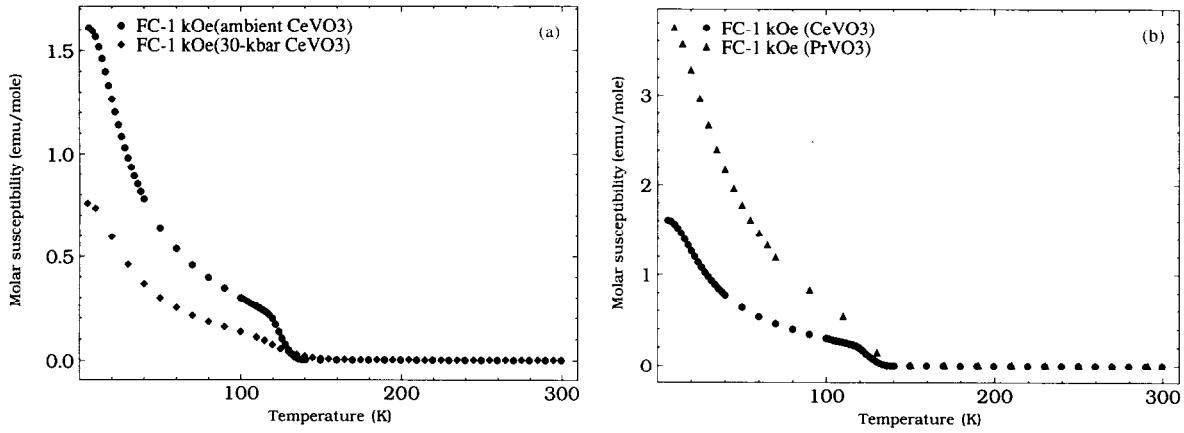


FIG. 9. Temperature dependence of the molar susceptibility after a FC-1 kOe of (a) $CeVO_3$ with two pressure syntheses and (b) $CeVO_3$ and $PrVO_3$.

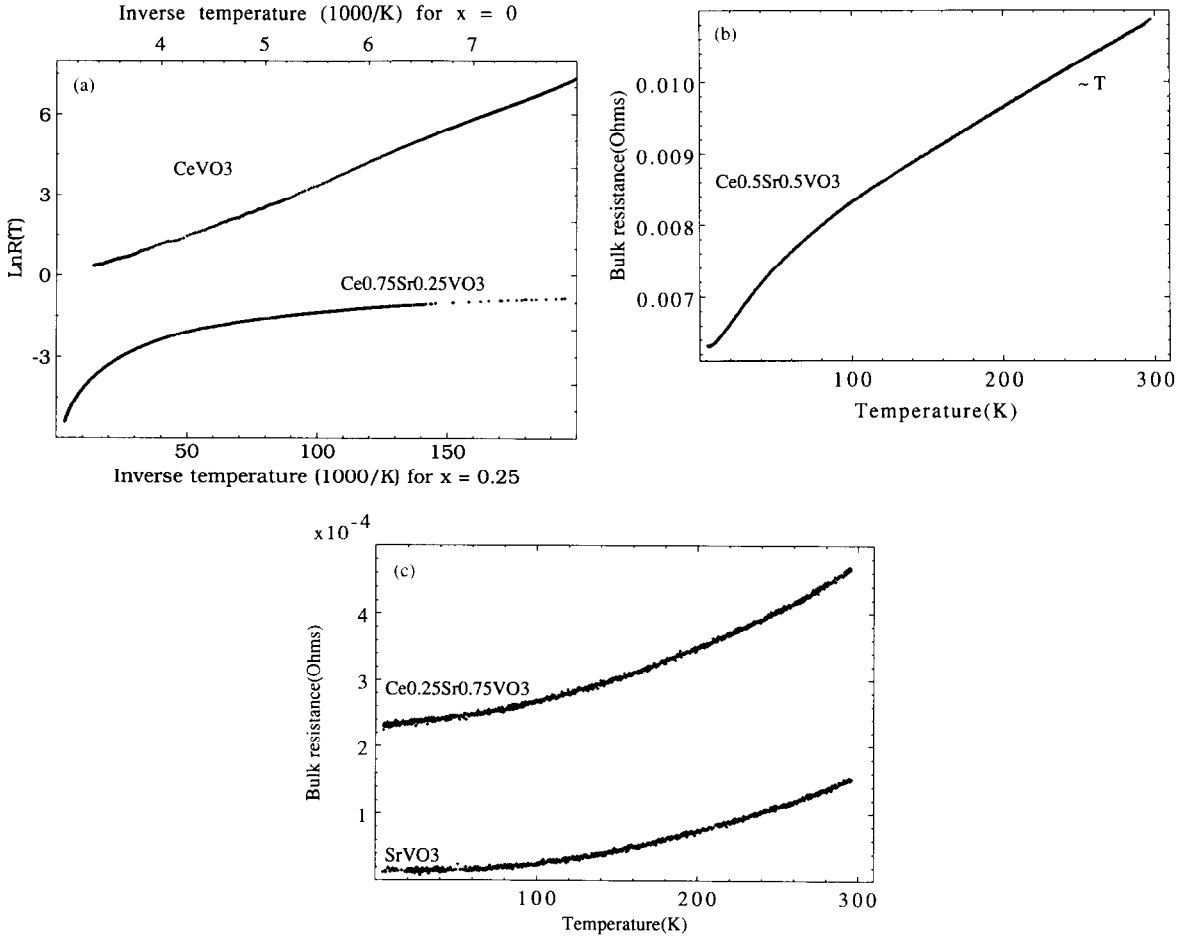


FIG. 10. (a) Logarithm of resistance versus inverse temperature of $CeVO_3$ and $Ce_{0.75}Sr_{0.25}VO_3$. Resistance versus temperature of (b) $Ce_{0.50}Sr_{0.50}VO_3$ and (c) $Ce_{0.25}Sr_{0.75}VO_3$ and $SrVO_3$.

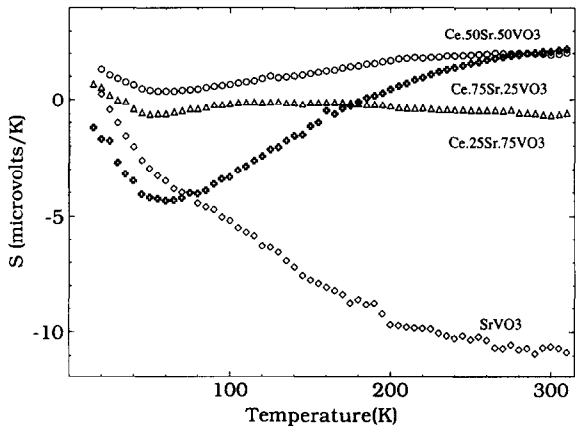


FIG. 11. Seebeck coefficient versus temperature of $Ce_{1-x}Sr_xVO_3$ with $0 \leq x \leq 0.1$.

ing the applied field from its maximum value to $H_N$. Recasting [4] as

$$(M_s + \chi_0 H - M)H^2 = aH + b \qquad [5]$$

and subtracting the term $\chi_0 H$ gives a linear plot from which the parameters $a$ and $b$ can be extracted. The constant $a$ is an extrinsic parameter that should vanish in a perfect crystal; for a cubic ferromagnet a $b = 0.0762\,(K_1/M_s)^2$ has been found. If $M_s$ is taken as the value of $M$ at $H = 50$ kOe, the values of $a$, $b$, $K_1$, and $\chi_0$ that result are given in Table 3. Chemical inhomogeneities associated with the distribution of Ce and La in $Ce_{0.5}La_{0.5}VO_3$ may be responsible for the large value of $a$ obtained for this material. Such inhomogeneities could also account for a rounding of the knee at $H_N$ since their presence would impede the motion of domain walls that are nucleated. On going from $Ce_{0.5}La_{0.5}VO_3$ to $CeVO_3$, the measured $M_s$ increases by about a factor 2, as would be expected if the Ce-atom moments $\mu_{Ce}$ were the dominant contributors to $M_s$; the parameters $b$ and $\chi_0$ increase by a factor 1.7, which implies an increase in the effective anisotropy constant of about a factor 2.6. The dramatic increase in $M_s$ with Ce doping can therefore account for the drop in $H_N$ on going from $LaVO_3$ to $Ce_{0.5}La_{0.5}VO_3$ according to Eq. [3].

Independent evidence that the magnetism of the $VO_3$ array of $CeVO_3$ behaves like that of $LaVO_3$ comes from the existence of a metastable high-pressure $CeVO_3$ phase. In both $LaVO_3$ and $CeVO_3$ there is a cooperative Jahn–Teller distortion that enhances the orbital angular momentum on cooling through a transition temperature $T_t < T_N$, and in both we find stabilization of a metastable high-pressure phase in which the cooperative Jahn–Teller distortion is suppressed. In the $LnVO_3$ perovskites with smaller $Ln^{3+}$ ions, there is no metastable high-pressure phase and no magnetostrictive distortion below a $T_t$. We have interpreted this correlation to be due to a first-order delocalization of the V-3$d$ electron with increasing pressure, hydrostatic for $Ln$ = La and Ce or chemical for smaller $Ln^{3+}$ ions. Metastable high-pressure $CeVO_3$ exhibits no anomalous behavior in its $\chi_m(T)$ curve, which remains smaller than that of stable $CeVO_3$ below $T_N$. A weak ferromagnetism of the $VO_3$ array having an $\mathbf{M}_V$ in the direction of $\mathbf{M}_{Ce}$ and $\mathbf{H}$ in the interval $T_t < T < T_N$ enhances the volume of material in stable $CeVO_3$ having its total magnetization aligned favorably with respect to an $H = 1$ kOe at all temperature $T < T_N$; in metastable $CeVO_3$ where the $VO_3$ array has no weak ferromagnetism, the volume of material having its magnetization aligned parallel to $\mathbf{H}$ below $T_N$ is relatively small.

Reversal of the sign of the weak ferromagnetism of the $VO_3$ array on cooling through $T_t$ in stable $CeVO_3$, though enhancing a break in $(d\chi_m/dT)$ at $T_t$, does not reverse the V–Ce exchange coupling operating on $M_{Ce}$ below $T_N$, so

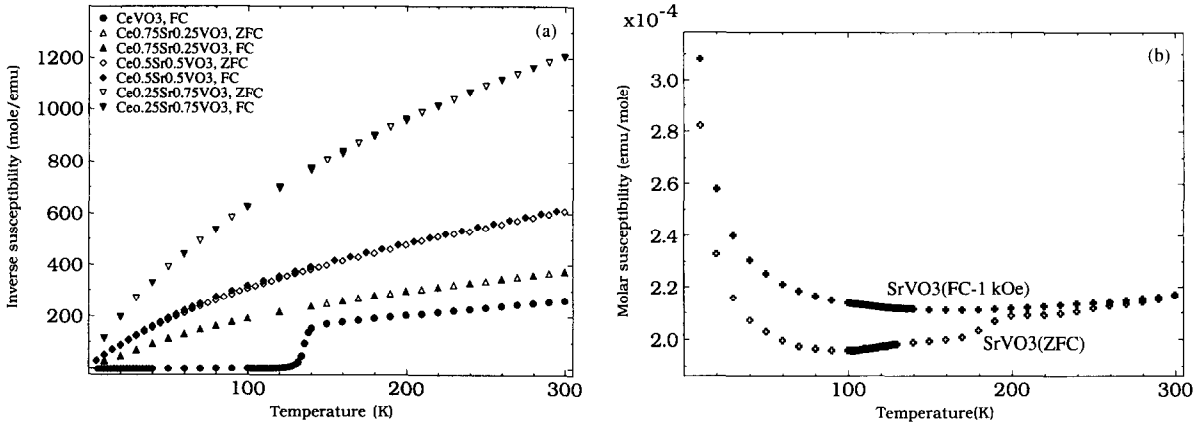


FIG. 12. (a) Inverse molar susceptibility as a function of temperature for $Ce_{1-x}Sr_xVO_3$ with $0 \leq x \leq 1$ and (b) temperature-dependent susceptibility of $SrVO_3$ measured in 1 kOe after ZFC and FC-1 kOe from room temperature to 4 K.

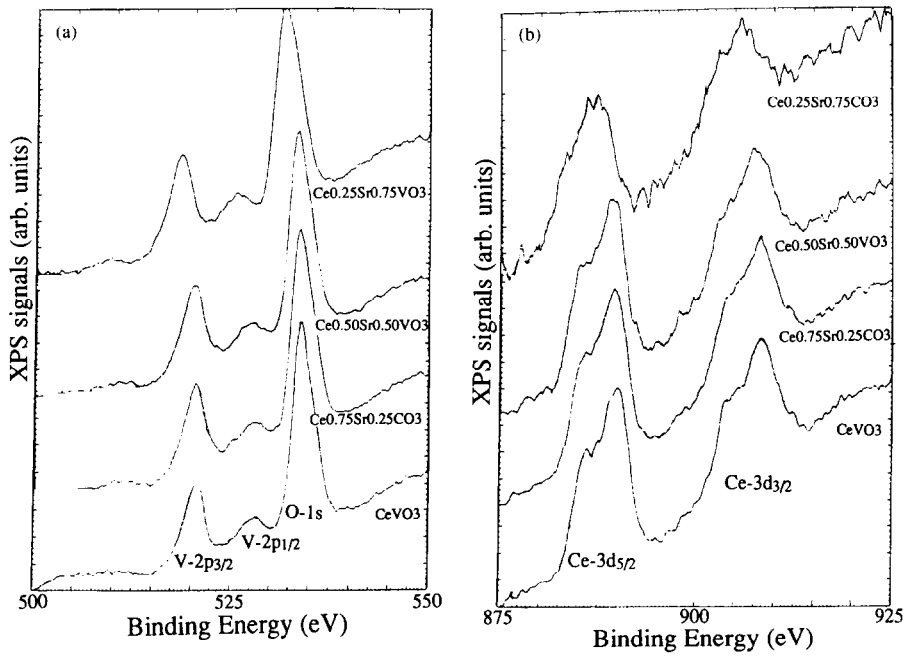


FIG. 13. X-ray photoelectron spectra as a function of the core binding energies for (a) V-2*p* and O-1*s* states and (b) Ce-3*d* states for $Ce_{1-x}Sr_xVO_3$ with $0 \leq x \leq 1$.

the $\chi_m(T)$ measured in 1 kOe remains higher in stable $CeVO_3$ than in metastable high-pressure $CeVO_3$. The enhanced ordering of the $\mu_{Ce}$ below 40 K in both samples indicates that the V–Ce exchange coupling is not changed significantly by the electronic transition induced by high pressure.

One of the factors that makes vanadium oxide chemistry so rich is its tendency to exhibit first-order transitions between more localized and more delocalized V-3*d* electrons. This tendency is illustrated not only by the stabilization of metastable high-pressure phases in $LaVO_3$ and $CeVO_3$, but also by the insulator–metal transitions found in the $Ln_{1-x}M_xVO_3$ perovskites, with $M$ = an alkaline earth.

*2. $Ce_{1-x}Sr_xVO_3$.* The volume of the unit cell decreases nonlinearly with increasing $x$ over the compositional range $0.25 \leq x \leq 0.75$ in the system $Ce_{1-x}Sr_xVO_3$, Table 1; it decreases linearly with $x$ in $La_{1-x}Sr_xVO_3$ for $0 \leq x < 1$ (9). This difference already indicates an oxidation of the Ce-atom array in the system $Ce_{1-x}Sr_xVO_3$.

We interpret the evolution of the transport and magnetic properties of the system $Ce_{1-x}Sr_xVO_3$ with the schematic energy diagram of Fig. 14. In the insulator $CeVO_3$, Fig. 14a, the Fermi energy $E_F$ lies above the $V^{4+}/V^{3+}: 3d^2$ and $Ce^{4+}/Ce^{3+}: 4f^1$ redox couples in an energy gap separating the empty $V^{3+}/V^{2+}: 3d^3$ couple from the localized occupied states responsible for the atomic moments; these redox couples lie in the energy gap between the valence bands of primarily O-2*p* parentage and the conduction bands of primarily V-4*s* and Ce-5*d* parentage.

The substitution of Sr for Ce lowers $E_F$ into the $Ce^{4+}/Ce^{3+}$ and $V^{4+}/V^{3+}$ couples; the holes so introduced into these couples may be either trapped as small polarons within the $Ce^{4+}/Ce^{3+}$ couple or form molecular-orbital (MO) states at the eight near neighbors of a Sr atom, Fig. 14b. The insulator–metal transition with increasing $x$ occurs where the percolation limit is reached for transition to a narrow $\pi^*$ band via vanadium atoms near neighbor to a $Sr^{2+}$ ion. Formation of a narrow $VO_3$-$\pi^*$ band at vanadium atoms near neighbor to a $Sr^{2+}$ ion is consistent with stronger V–O bonding at higher-valence vanadium, which would stabilize the more delocalized V-3*d* states found in metastable, high-pressure $CeVO_3$. With this model, the system would exhibit variable-range hopping and/or small polarn motion in compositions $0 < x < 0.25$ with a transfer of spectral weight from the $V^{4+}/V^{3+}$ couple to the gap in excess of one state per Sr atom. In the range $0.25 < x \leq 0.50$, where $x$ exceeds the Sr-atom percolation threshold, a partially occupied $\pi^*$ impurity band is formed in which $E_F$ is pinned at the $Ce^{4+}/Ce^{3+}$ couple of the remaining Ce atoms. This situation results in a classical intermediate-valence state at the Ce atoms, valence fluctuations between the $Ce^{4+}/Ce^{3+}$ couple and the MO or band states of the partially filled lower Hubbard band being associated with a strong hybridization of Ce-4*f* and near-neighbor V-3*d* states. Already by $x = 0.5$, the hybrid-

TABLE 3
Coercive Field $H_c$, Remanence Field $B_r$, the Differential Susceptibility of Reversible Rotation of Hysteresis $\chi_0 = (dM/dH)_{rev}$, and Constants $a$, $b$, $K_1$ of the $Ce_{1-x}La_xVO_3$ Measured at 20 K after ZFC

| Samples | $H_c$ (kOe) | $B_r$ (emu/g) | $\chi_0$ ($10^{-5}$ emu/g · Oe) | $a$ (Oe) | $b$ ($10^6$ Oe$^2$) | $K_1$ ($10^4$ erg/ccm) |
|---|---|---|---|---|---|---|
| $LaVO_3$ | ≈0.0 | ≈0.0 | 0.06 | | | |
| $Ce_{0.5}La_{0.5}VO_3$ | 6.34 | 2.76 | 0.36 | 1938 | 1.89 | 1.49 |
| $CeVO_3$ | 3.98 | 5.72 | 0.61 | 651 | 3.26 | 3.85 |

ization suppresses the localized character of the Ce-4*f* electrons at lowest temperatures and hence any magnetic order.

By $x = 0.75$, the less than half-filled $V^{4+}/V^{3+}$ "lower Hubbard band" dominates the Seebeck voltage at lowest temperatures, but hole conduction in the $Ce^{4+}/Ce^{3+}$ couple appears to contribute significantly at higher temperatures, Fig. 11.

In the absence of Ce atoms, stoichiometric $SrVO_3$ exhibits the transport properties of a typical metal; the V–O–V interactions are strong enough to create ($\frac{1}{8}$)-filled $\pi^*$ bands. However, the $\pi^*$ bands remain sufficiently narrow that the electrons stabilize an itinerant electron antiferromagnetic spin-density wave with a canted-spin ferromagnetism near the stoichiometric composition corresponding to all $V^{4+}$ ions. The on-site electron correlations are most strongly manifest in a single-valent compound where the Hubbard model applies. Removal of oxygen induces a first-order phase change between weakly correlated electrons in the $\pi^*$ band of $SrVO_{2.9}$ and strongly correlated $\pi^*$ electrons in $SrVO_3$.

The XPS data of Fig. 13 and Table 2 are consistent with a delocalization of the V-3*d* electrons on doping and a valence fluctuation at the Ce atoms that is fast relative to $10^{-5}$ sec.

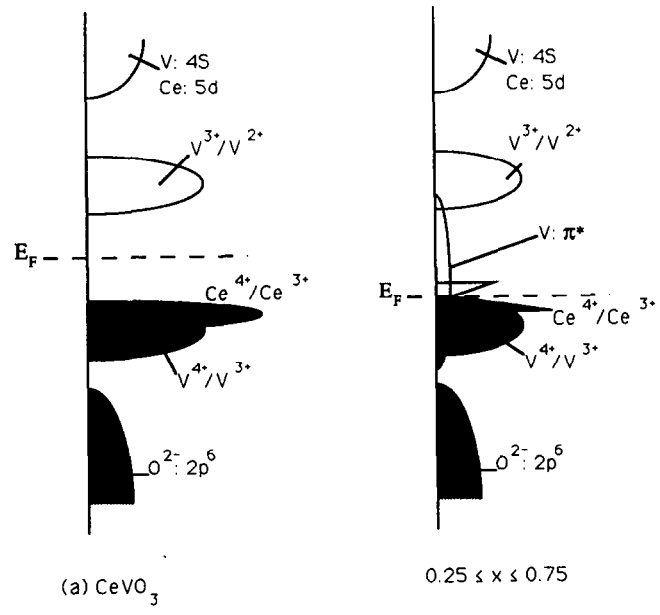


FIG. 14. Schematic density of states versus energy diagram for (a) $CeVO_3$ and (b) $Ce_{1-x}Sr_xVO_3$ with $0.25 \leq x \leq 0.75$. The V-$\pi^*$ band is associated with V atoms having a Sr near neighbor.

## CONCLUSIONS

The perovskite $CeVO_3$ has a $VO_3$ array that behaves like the $VO_3$ array of $LaVO_3$. In $LaVO_3$, long-range antiferromagnetic order with a canted-spin ferromagnetic component sets in at $T_N \approx 142$ K; in $CeVO_3$ the same magnetic order of the $VO_3$ array sets in at $T_N \approx 136$ K. Both compounds undergo a first-order magnetostrictive distortion at a $T_t < T_N$; we find $T_t \approx 138$ K in $LaVO_3$ and 124 K in $CeVO_3$. The transition is due to a cooperative Jahn–Teller distortion that removes the orbital degeneracy of the localized $V^{3+}: t^2e^0$ configurations in a way that enhances the orbital angular momentum; the orbital angular momentum increases discontinuously on cooling through $T_t$. In the presence of a strong intraatomic spin-orbit coupling, such a cooperative transition is made possible by the long-range ordering of the $V^{3+}$-ion spins. Also, in both perovskites high-pressure synthesis stabilizes a metastable, isostructural phase below 250°C, in which the magnetostrictive distortion at $T_t$ is suppressed. Suppression of the magnetostrictive, localized-electron Jahn–Teller distortion by pressure is attributed to a first-order change in the extent of V–O 3*d*–2*p* covalent mixing and hence of the delocalization of the V-3*d* electrons. With smaller $Ln^{3+}$ ions in the $LnVO_3$ perovskites, bond-length mismatch exerts a compressive stress on the $VO_3$ array that suppresses the cooperative Jahn–Teller magnetostrictive distortion.

The vanadium atomic moments $\mu_V$ have been shown to reverse their direction on cooling/heating through $T_t$ in $LaVO_3$; we have presented indirect evidence in this paper that the vanadium moments $\mu_V$ also change direction in $CeVO_3$ on thermally traversing $T_t$, but without inverting the sign of the V–Ce exchange field at the Ce

atoms. Inversion of the direction of each $\mu_V$ on traversing $T_t$ has been attributed to the discontinuous change in the orbital angular momentum, which induces a persistent atomic current in a direction to oppose an applied or exchange field at the vanadium atom. Retention of the sign of the V–Ce exchange field through $T_t$ indicates that the interaction is antisymmetric with an exchange field at the Ce atoms of the form of Eq. [2].

The V–Ce interatomic exchange field is manifest in the magnetic susceptibility $\chi_m(T)$ by a sharp increase in the magnetization $\mathbf{M} = \chi_m \cdot \mathbf{H}$ on cooling through $T_N$ in a constant applied field $\mathbf{H}$ and also the opening of an $M$–$H$ hysteresis loop below $T_t$ that is not found in $LaVO_3$ in excursions of $H$ to $\pm 50$ kOe. A sharp change in $d\chi_m/dT$ at $T_t$ is attributed to a reversal of the direction of each $\mu_V$ (as well as to a dramatic change in the magnetocrystalline anisotropy) and retention of the direction of the Ce-atom magnetization. A rapid increase with decreasing temperature in the magnetization $M = \chi_m \cdot H$ below 40 K reflects an ordering of the Ce-atom moments; a reorientation of the Ce-atom moments seems to occur at a $T_s \approx 4$ K.

Three aspects of the system $Ce_{1-x}Sr_xVO_3$ are of interest. First, the substitution of $Sr^{2+}$ for $Ce^{3+}$ oxidizes both the cerium and vanadium atoms, which makes the evolution of the lattice parameters with $x$ deviate strongly from Végard's law, as can bee seen from Table 1. Second, oxidation of the vanadium $x \geq 0.25$ does not result in small-polaron $V^{4+}$ ions, but in a delocalization of the V-3$d$ electrons as prefigured by a metastable high-pressure phase; at small $x$, delocalized molecular orbitals are created nonadiabatically at the cluster of 8 near-neighbor V atoms of an isolated $Sr^{2+}$ ion, and at larger $x$, percolation allows creation of itinerant electron $\pi^*$ band states. The transition from localized $V^{3+}: t^2e^0$ configurations to delocalized states transfers excess spectral weight into the energy gap between $V^{4+}/V^{3+}$ and $V^{3+}/V^{2+}$ couples, and hybridization of Ce-4$f$ and V-3$d$ states at $E_F$ creates intermediate-valence fluctuations at the Ce atoms and suppresses the Ce atomic moments at low temperatures. Third, stoichiometric $SrVO_3$ exhibits magnetic ordering at low temperatures; the strong on-site electron correlations inhibit charge transfer in the stoichiometric compound, stabilize itinerant-electron magnetism, and also increase the volume.

## ACKNOWLEDGMENTS

The authors thank the NSF, the Robert A. Welch Foundation, Houston, Texas, and the Texas Advanced Research Program for support of this work.

## REFERENCES

1. V. G. Zubkov, G. V. Brazuev, and G. P. Shveikin, *Sov. Phys. Solid State* **18,** 1165 (1976).
2. A. S. Borukhovich, G. V. Brazuev, and G. P. Shveikin, *Sov. Phys. Solid State* **15,** 1467 (1974); **16,** 181 (1974).
3. P. Bordet, C. Chaillout, M. Marezio, Q. Huang, A. Santoro, S.-W. Cheong, H. Takagi, C. S. Oglesby, and B. Batlogg, *J. Solid State Chem.* **106,** 253 (1993).
4. Q. Huang, A. Santoro, P. Bordet, M. Marezio, S.-W. Cheong, and B. Batlogg, private communication, 1993.
5. E. F. Bertaut, *in* "Magnetism: A Treatise on Modern Theory and Materials" (G. T. Rado and H. Suhl, Eds.), Chap. 4. Academic Press, New York, 1963.
6. J. B. Goodenough and H. C. Nguyen, *C. R. Acad. Sci., Paris,* **319,** 1285 (1994).
7. H. C. Nguyen and J. B. Goodenough, *Phy. Rev. B* **52,** 335 (1995).
8. J. B. Goodenough and J. Zhou, *Phys. Rev. B* **47,** 5275 (1993).
9. A. V. Mahajan, D. C. Johnston, D. R. Torgeson, and F. Borsa, *Phys. Rev. B* **46,** 10973 (1992).
10. P. de la Mora and J. B. Goodenough, *J. Phys. C.* **20,** 3391 (1987).
11. J. B. Goodenough and J. M. Longo, Eds., "Magnetic and Other Properties of Oxides and Related Compounds," p. 126, Landolt–Borenstein Numerical Data and Functional Relationships in Science and Technology, New Series, Group 3, Vol. 4, Pt. A (K. H. Hellwege, Ed.). Springer-Verlag, Berlin/New York, 1970.
12. R. Grossinger, *in* "Proceedings of the International Workshop 'Magnetism, Magnetic Materials and Their Applications' " (F. Leccabue and J. L. Sanchez, Eds.), Sect. 1, pp. 3–11. Llamzares, Havana, Cuba, May 21–29, 1991.
13. H. Kronmuller, "Supermagnets, hard magnetic materials" (G. I. Long and F. Grandjera, Eds.), Chap. 19. Kluwer Academic, Dordrecht, 1991.
14. P. Weiss, *J. Phys.* **6,** 667 (1907).
15. S. Chikazumi, "Physics of Magnetism," Chaps. 11, 12. Krieger, Melbourne FL, 1978.
16. E. Czerlinsky, *Ann Phys.* **13,** 80 (1932).
17. L. Néel, *J. Phys. Radium* **9,** 184 (1948).
18. T. Shishido, H. Iwasaki, N. Toyota, M. Tanaka, H. Horiwachi, S. Nojama, S. Nakagawa, and T. Inkuda, *J. Alloy Comp.* **209,** L11 (1994).
19. E. Parazzo, *Surf. Sci.* **234,** L 253 (1990).
20. J. W. Allen, *J. Magn. Magn. Mater.* **47, 48,** 160 (1985).
21. C. A. Strydom and H. J. Strydom, *Inorg. Chim. Acta* **161,** 7 (1989).
22. G. A. Sawatzky and D. Post, *Phys. Rev. B* **30,** 1546 (1979).